High-Speed Path Tracking of a Small Mobile Robot Using PD and ADRC Controllers with Experimental Validation

Pasan Senarath[1] , K. Jayawickrama C. Kumara[2]
[1]Department of Electrical and Electronics Engineering
[2]Department of Mechanical Engineering
Faculty of Engineering, Sri Lanka Institute of Information Technology
senarathpasan@gmail.com , Kumara.j@sliit.lk

ABSTRACT

This paper presents the development, modeling, and validation of a compact ground-based mobile robot designed for high-speed trajectory tracking with low-cost hardware and advanced control strategies. Originally designed for micromouse competitions, the platform was upgraded with a vacuum-assisted friction enhancement mechanism and a lightweight sensor fusion system comprising Time-of-Flight (ToF) sensors, infrared (IR) proximity sensors, a 6-axis IMU, and wheel encoders. Due to the lack of manufacturer-provided system parameters, a data-driven system identification approach was employed to derive a MIMO state-space model representing the robot's dynamics. Two control strategies, Proportional-Derivative (PD) and Active Disturbance Rejection Control (ADRC) were implemented and evaluated through both numerical simulations and real-world experiments across three benchmark trajectories: straight-line, 90° smooth turn, and figure-eight. The results show that both controllers achieved trajectory tracking within 5% RMSE, with ADRC offering improved heading accuracy and energy efficiency. Experimental observations indicate that ADRC reduces battery current fluctuations, although current modeling was not included in the control design. The proposed platform and methodology offer a cost-effective and robust solution for mobile robot control in constrained environments, with future work focusing on energy-aware control integration.

Keywords: *Mobile Robot, System Identification, PD Controller, ADRC, Sensor Fusion, Vacuum Traction*

INTRODUCTION

Small ground-based mobile robots, particularly differential-drive platforms originally designed for micromouse competitions, have attracted growing interest for applications in indoor inspection, swarm coordination, and educational robotics. These platforms offer advantages in cost, accessibility, and maneuverability in constrained spaces. However, achieving high-speed ($\geq$ 1 m/s) and high-precision motion remains challenging when relying on off-the-shelf components that lack well-characterized dynamics (Ušinskis, Nowicki, Dzedžickis, & Bučinskas, 2025). Model-based control traditionally depends on accurate mechanical and actuator parameters, yet low-cost motors and mechanical tolerances in small platforms introduce variability that undermines performance. This impedes the application of classical controllers in transitioning from simulations to real-world settings (Norzalilah & Samad, 2023). A particularly novel aspect of our work is the integration of a vacuum-based friction enhancement, a lightweight and low-power method increase normal force, thereby improving traction during aggressive maneuvers. While vacuum adhesion is well-established in wall-climbing robotics, its application to planar traction control in fast-moving ground robots is largely unexplored (Yuan, Chang, Song, Lin, & Jing, 2024). Furthermore, sensor fusion strategies using IMU, Time of Flight sensors and infrared (IR) sensors have shown promise in localization and navigation (Ušinskis et al., 2025), but their deployment in high-speed miniature platforms is under-investigated. Fusion of simple, low-cost sensors offers a feasible alternative to bulkier systems such as LIDAR or stereo vision (Ušinskis et al., 2025). In terms of control architectures, while Proportional-Derivative (PD) and Active Disturbance Rejection Control (ADRC) are well-studied in theory, practical benchmarks on physical, small-scale robots navigating curves and complex trajectories at high speeds remain scarce (Muñoz-Hernandez, Díaz-Téllez, Estevez-Carreon, & García-Ramírez, 2023).
This paper presents:

A compact $60 \times 40 \times 25$ mm differential-drive robot, modified with a vacuum-assisted downforce mechanism to mitigate wheel slip.

A sensor fusion system combining IR and IMU data for real-time obstacle avoidance and heading estimation.

A data-driven system identification approach for straight and curved motions, enabling adaptive control.

Comparative experimental validation of PD and ADRC controllers in simulation and on real hardware, demonstrating precise path-following (> 1 m/s) on straight lines and figure-eight trajectories.

Together, these contributions address critical gaps in model identification, friction control, sensor fusion, and

https://doi.org/10.54389/HMVX6558

control validation for high-performance small mobile robots. The results point to substantial potential for deploying such platforms in inspections, swarm systems, and competitive robotics.

MATERIALS AND METHODS

This section outlines the development process of the compact mobile robot platform, the sensor and actuation systems, the system identification procedure, and the control algorithm implementation (PD and ADRC). The methodology is structured in sequential stages to align with standard practices in mobile robotics research, integrating novel hardware and rigorous control implementation.

Robot Platform and Hardware Configuration

The mobile robot measures $60 \times 40 \times 25$ mm and utilizes a four-wheeled differential-drive setup built from low-cost components. The chassis is implemented on the PCB itself, balancing rigidity and lightweight design. Key components:

Actuators and gear system: Two 0714 coreless motors, customized motor mount, gear system, tires, rims, bearings for differential drive.
Sensing system: Time of flight sensors (infrared sensors) for obstacle proximity detection (front and sides), magnetic encoders, inertial measurement unit (IMU) for heading angle and linear acceleration feedback.
Friction Control Mechanism: A miniature coreless motor-driven fan positioned beneath the chassis generates a vacuum skirt to enhance downward force, improving wheel grip during rapid turns and linear motion.
Processing and Control: A microcontroller unit (ESP32S3PICO) is used for data acquisition, motor control, and executing control algorithms.
Motor drivers and power supply: Two motor drivers and 3.3V step down buck converter, two 1S 150 mAh LiPo cells connected in series (2S, 7.4 V, 150 mAh) to power the robot.

Figure 1 shows an annotated hardware diagram of the mobile robot from top and bottom views.
System Identification Procedure
Precise dynamic parameters were not available from the off-the-shelf components. A data-driven system identification was conducted to obtain accurate motion models, aligning with recent methods in differential-drive robotics (Guffanti et al., 2025; Siwek et al., 2023).

Experimental Setup and Data Acquisition

Two motion profiles under open-loop control were executed: (a). Straight-line motion for identifying translational dynamics. (b). Known left-turn motion for angular response identification. In both cases, a unit-step PWM command (0–255) was issued to the motor driver via the microcontroller, while position, velocity, and heading data were recorded at 100 Hz without any active control algorithm. Sensor data was processed offline to estimate key dynamic variables (velocity, acceleration, heading angle). Noise filtering and low-pass filtering were applied to improve signal quality. The vacuum system was operated at a constant power level throughout all tests. At the tested speeds, wheel slip was considered negligible, as the vacuum-generated downforce provided sufficient traction to counteract potential slipping forces.

Transfer Function Derivation and Modelling

Using input-output data from both motion types, system transfer functions were derived through curve fitting and regression using python library system identification toolchain. Figure 2 illustrates the system identification block diagram. Individual transfer functions for each motor and simplified linear velocity and angular velocity models were obtained following Guffanti et al. (2025). The identified model served as the baseline for controller design. Using this method, the robot was modeled as a simplified 2-input, 2-output (MIMO) system.

Control Algorithm Design

Two controllers were implemented based on the identified model: Proportional-Derivative and Active Disturbance Rejection Control. The following sub-sections describe the details of the control algorithm design.

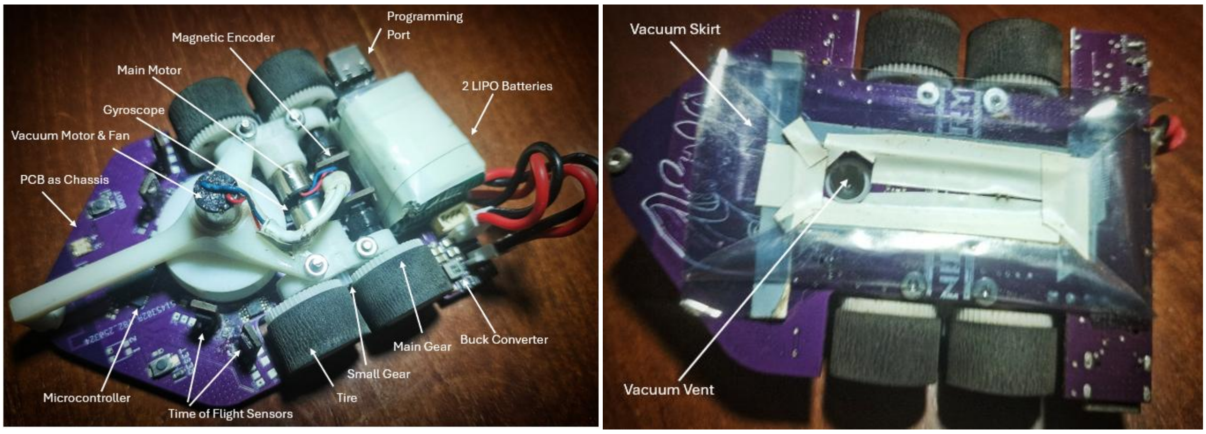

Figure 6. Mobile robot platform

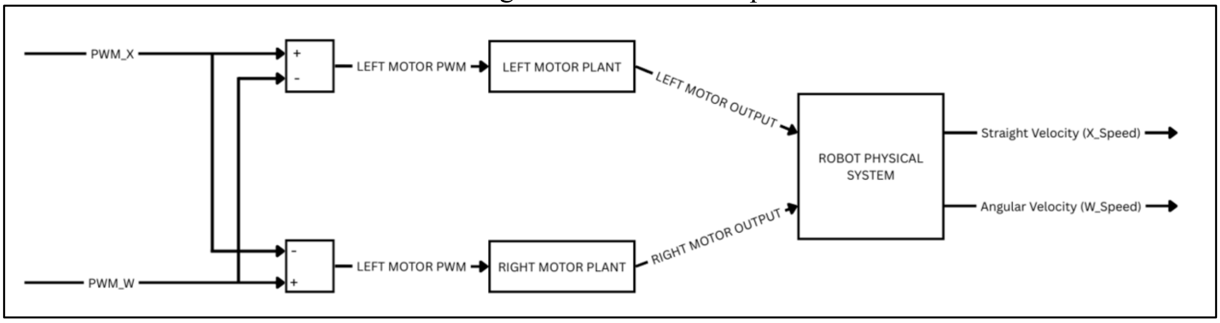

Figure 2. Block diagram of the system identification process.

Proportional-Derivative (PD) Controller

A standard Proportional-Derivative (PD) controller was implemented to regulate the heading angle and position of the mobile robot. The control law is defined in Equation (1):

$$u(t) = K_p e(t) + K_d \frac{de(t)}{dt} \quad (1)$$

where $e(t)$ represents the instantaneous error (in position or heading), and K_p and K_d are the proportional and derivative gains, respectively.

Gains were empirically tuned using step-response data obtained from the identified model. The tuning objective was to achieve fast settling time, minimal overshoot, and adequate stability. This approach follows well-established procedures in robotic path tracking (Hussein & Al-Khafaji, 2022) and has proven effective in similar mobile robot applications (Wu & Cao, 2011).

Active Disturbance Rejection Control (ADRC)

The successful use of ADRC in two-wheeled and differential-drive mobile robots has been demonstrated in several recent studies (Muñoz-Hernandez et al., 2023; Wu & Cao, 2011), confirming its applicability to real-world mobile robotic systems with limited sensing and actuation precision. To improve robustness against modeling uncertainties and unmeasured disturbances (such as wheel slip, friction variation, and external forces), an Active Disturbance Rejection Control (ADRC) framework was implemented for both linear and angular velocity regulation. The ADRC controller is composed of three primary components:

Tracking Differentiator (TD): This module smooths the reference input signal and estimates its derivative, enabling better transient performance. It mitigates discontinuities in setpoints and prepares the system for fast response without overshooting.

Extended State Observer (ESO): ESO is the core innovation of ADRC. It estimates both the unmeasured system states and the total disturbance (internal + external), treating the entire unknown dynamics and perturbations as an extended state. This enables real-time compensation and enhances tracking accuracy (Han, 2009; Wu & Cao, 2011).

Nonlinear State Error Feedback (NLSEF): Instead of traditional linear gains, ADRC employs nonlinear gain functions (e.g., fal or sigmoid) to adjust control effort based on the magnitude of the error. This improves control precision near steady-state and limits aggressiveness when errors are large. The control law is defined by the equation (2) as:

$$u(t) = u_0(t) - \hat{f}(t) \tag{2}$$

where: $u(t)$ is the control input to the system, $u_0(t)$ is the output of the nonlinear feedback control law, and $\hat{f}(t)$ is the real-time estimated total disturbance from the ESO.

The robot's MIMO system (PWM_X → Speed_X, PWM_W → Speed_W) was controlled using two separate ADRC loops—one for linear and another for angular velocity. Each loop used a second-order ESO based on the estimated state-space model from system identification. Controller tuning followed the guidelines established in the literature (Han, 2009), where the observer bandwidth $\omega_0(t)$ was set 3–5 times higher than the controller bandwidth $\omega_C(t)$ to ensure fast and accurate disturbance estimation. Parameter tuning was refined empirically based on the observed transient response. This ADRC approach allows the robot to track paths accurately even under varying loads or floor conditions, maintain heading stability at high speeds (up to 1.2 m/s), and reject unmodeled disturbances without requiring an exact plant model.

Sensor Fusion

Low-cost infrared (IR) and inertial measurement unit (IMU) sensors were integrated to provide robust state estimation for both obstacle detection and heading control—key requirements for indoor mobile robot deployment. Four multi-directional IR modules provide range measurements for nearby obstacles and path boundary detection. A 6-axis IMU records angular velocity and linear acceleration to estimate orientation and motion dynamics. Encoders are used as a supplement to the IMU for odometry to improve drift correction. Fusion reduced IMU drift and corrected heading using encoder updates, yielding average errors of less than 1° over 10 m trajectories. For obstacle detection, the fused IR sensors reliably detected nearby objects at approximately 0.2 m, enabling timely avoidance actions. Overall, the fusion approach delivered a lightweight, cost-effective solution for indoor navigation, significantly enhancing pose estimation and environmental awareness without requiring expensive sensors like LiDAR or vision systems.

NUMERICAL SIMULATIONS

Numerical simulations were conducted using the empirically identified state-space model and implemented control laws—PD and ADRC. The robot's performance was evaluated on three motion profiles designed to reflect typical navigation maneuvers: straight-line traverse, smooth 90° turn and figure-eight trajectory. To isolate the performance of the control algorithms, obstacle avoidance and proximity sensing were disabled. Feedback was limited to the IMU and wheel encoders, aligning with the physical robot's available sensory inputs. This approach ensured consistent comparison between simulation and experiment. Two simulation block diagrams were created, as shown in Figures 3 and 4. The figure-eight trajectory was designed with a diameter of approximately 144 mm per loop and was chosen to evaluate both curvature handling and heading correction. Similar simulation-based evaluation of mobile robot controllers has been reported in recent studies using figure-eight paths for benchmarking (Masalskyi et al., 2024; Muñoz-Hernandez et al., 2023; Guffanti et al., 2025). The controller performance of PD and ADRC were assessed using 3 key metrics viz position tracking error (RMSE) and heading angle deviation. Results are visualized in section 3.

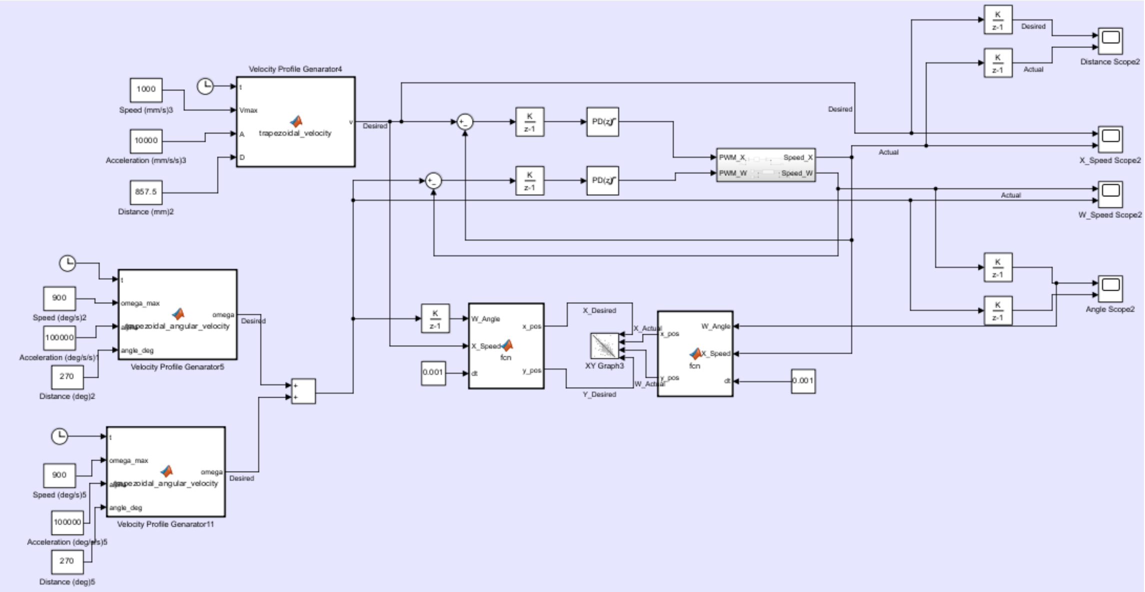

Figure 3. PD control—figure-eight simulation

PHYSICAL EXPERIMENTS

After validating both controllers in simulation, the same path scenarios were recreated in the physical environment using a custom printed track setup. The robot was evaluated on straight-line track (2.5 m), a smooth 90° arc (radius: 75 mm) and figure-eight trajectory (144 mm loops). During experiments, the vacuum-assisted traction system was activated with a constant speed (that is proportional to the vacuum force/grip) to maintain grip and reduce wheel slip at higher speeds. The robot reached speeds of up to 1.2 m/s, even during curved motion, without significant drift. Sensor fusion used only the IMU and encoders, as in simulation. The robot was evaluated based on the four experimental metrics such as RMSE of position against planned trajectory, heading angle error and slip observations. Data were recorded and plots were obtained in offline mode. The results were compared to simulation data and validated using figures for visual correlation.

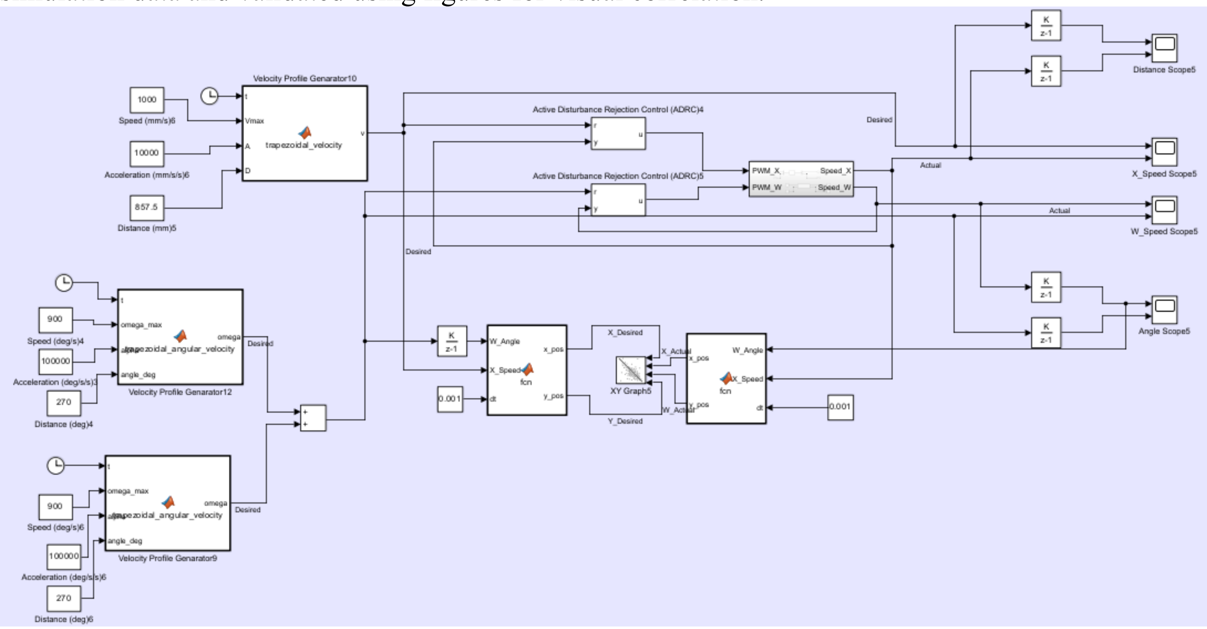

Figure 4. ADRC control—figure-eight simulation

Similar simulation and real-world validation of mobile robot controllers—particularly on bounded or printed figure-eight tracks—have been widely reported in recent research. For example, Masalskyi et al. (2024) and Ušinskis et al. (2025) conducted both simulation-based evaluations and physical experiments using indoor test paths to benchmark sensor fusion accuracy and navigation performance. Likewise, Guffanti et al. (2025) emphasized the role of simulation in modeling traction and slip dynamics, which were later validated through controlled physical trials to assess control reliability at elevated speeds.

RESULTS AND DISCUSSION

This section presents the results of the system identification, state-space modeling, and control validation stages of the mobile robot development. The findings directly support the study's primary objectives: to accurately model a small, low-cost mobile robot using experimental data, and to validate both classical (PD) and modern (ADRC) controllers through simulation and physical trials.

System Identification Results

Due to the absence of reliable modeling parameters from the low-cost, off-the-shelf components (e.g., motors, chassis, and drive systems), analytical modeling was impractical. Instead, a data-driven system identification approach was used to derive a state-space representation of the robot's dynamics. Controlled input signals (unit step PWM commands for translational and rotational drive) were applied to the motors, and the resulting output responses—linear velocity and angular velocity—were recorded using IMU and encoder feedback. Figure 5 illustrates the input signal as PWM value (0 to 255 scale) and output motor speeds measured by encoders in mm/s for the straight-line scenario. Figure 6 shows the input signal as PWM value (0 to 255 scale) and output robot rotational speed ω in mm/s for the 90 degrees smooth turn.

From these time-domain responses, transfer functions and a standard-form discrete-time identified state-space (SS) model were derived (Equation 3). This MIMO model treats the robot as a 2-input, 2-output system, with inputs as PWM signals and outputs as measured velocities. "Coefficient matrices A, B, C, and D were derived, with D consisting entirely of zeros.

$$\begin{aligned} \dot{x}(t) &= Ax(t) + Bu(t) + Ke(t) \\ y(t) &= Cx(t) + Du(t) + e(t) \end{aligned} \tag{3}$$

where $x(t)$is the state vector (position, speed, acceleration), $u(t)$ is the input vector ($[PWM\_X \quad PWM\_\omega]^T$, $y(t)$ is the output vector $[Speed\_X \quad Speed\_\omega]^T$ and $e(t)$ is the error matrix.

$$A = \begin{bmatrix} 0.9745 & 0.1683 & 0 & 0 & 0 & 0 \\ -0.1683 & 0.9745 & 0 & 0 & 0 & 0 \\ 0 & 0 & 0.8955 & 0.1662 & 0 & 0 \\ 0 & 0 & -0.1662 & 0.8955 & 0 & 0 \\ 0 & 0 & 0 & 0 & 0.9837 & 0.003119 \\ 0 & 0 & 0 & 0 & -0.003119 & 0.9837 \end{bmatrix}$$

$$B = \begin{bmatrix} -6.576 \times 10^{-5} & -1.348 \times 10^{-5} \\ -6.521 \times 10^{-5} & -3.763 \times 10^{-5} \\ -7.861 \times 10^{-4} & 1.191 \times 10^{-4} \\ 6.796 \times 10^{-5} & -4.759 \times 10^{-4} \\ -2.224 \times 10^{-5} & -1.343 \times 10^{-4} \\ -1.005 \times 10^{-4} & 3.36 \times 10^{-5} \end{bmatrix} \quad C = \begin{bmatrix} 1318 & 98.84 & 108.9 & -69.44 & -5574 & -1898 \\ 79.5 & -163.2 & 411 & 838.1 & -3369 & 1852 \end{bmatrix}$$

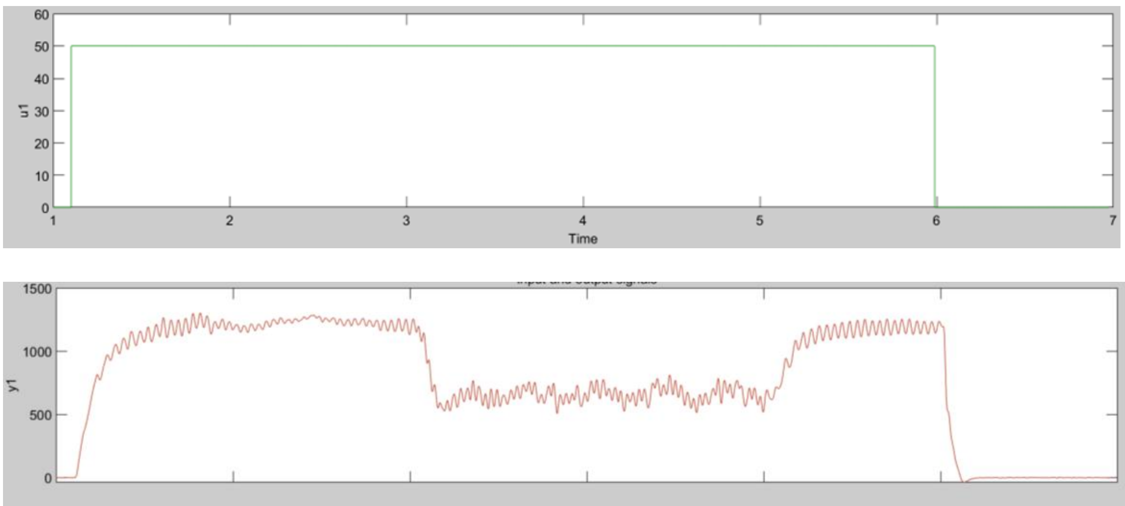

Figure 5. Input (top)-output (bottom) plots for translational motion (PWM_X → Speed_X)

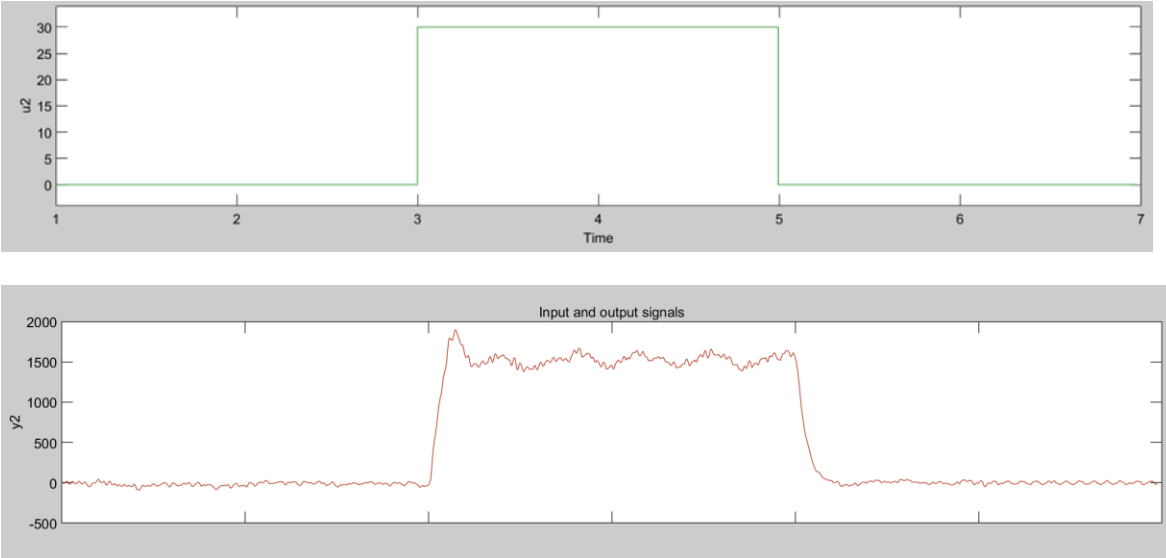

Figure 6. Input (top)-output (bottom) plots for rotational motion (PWM_W → Speed_ω)

This identification method compensates for the lack of component datasheets or manufacturer specifications by producing an experimentally grounded model. It serves as a reliable foundation for controller design (PD and ADRC), simulation-based trajectory testing and physical implementation and benchmarking in real-world conditions. The consistency between simulated and experimental results further validates the accuracy of this modeling approach—an essential outcome, given the hardware limitations. These results strongly align with the overall research objectives: developing an accurate, reliable control framework for a small mobile robot using data-driven modeling techniques, ensuring performance even under uncertainty and component variability.

SIMULATION AND EXPERIMENTAL RESULTS.

To evaluate the performance of both the PD and ADRC controllers, computer simulations and experiments were conducted using the identified state-space model for three representative motion profiles: straight-line motion, smooth 90° turn, and a figure-eight trajectory. The control inputs in all cases were PWM signals for translational and rotational motion, while the outputs were the corresponding linear velocity (Speed_X) and angular velocity (Speed_ ω).

The results are illustrated in Figure 7 and Figure 8 for PD controller and Figure 9 and Figure 10 for ADRC, each containing plots of control input commands and output speed responses for both translational and rotational components. Figure 8 and Figure 10 display the results for the figure eight trajectory, which involves alternating left and right turns. The PD controller can follow the path with acceptable accuracy, though small oscillations are visible in the angular velocity response. Figure 8 presents the response for the figure-eight trajectory. The ADRC controller maintains better trajectory adherence, reduced overshoot, and more consistent velocity tracking through the transitions between loops. Figure 11 and Figure 12 shows the battery current profile for both PD and ADRC controllers which are important in designing the power circuits and optimize the energy use in the mobile robot.

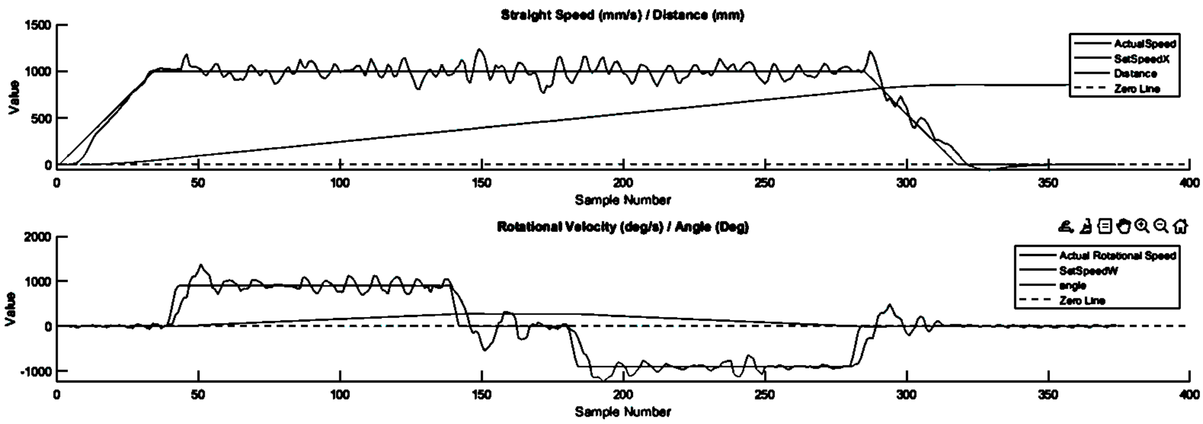

Figure 7. PD controller – (top) Straight Speed (bottom) Angular Speed

DISCUSSION

The performance of the PD and ADRC controllers was evaluated through both numerical simulations and physical experiments. The assessment focused on two key control metrics: position tracking error (RMSE) and heading angle deviation. Additionally, battery current consumption was measured during each test as a practical indicator of controller efficiency and energy performance, even though it was not included in the initial modeling. For all three test trajectories (straight path, 90° turn, and figure-eight), simulation results were used as the desired trajectory references. These references were then compared with actual paths recorded via encoder and IMU data during physical trials. Overall, both PD and ADRC controllers performed satisfactorily in reproducing the desired motion profiles: Position tracking RMSE remained within 5% of path length across all trials. Maximum heading deviations in physical tests reached up to 41% relative to simulated headings, particularly in the more aggressive transitions of the figure-eight path. These deviations were expected, as the simulation did not include certain physical factors such as motor backlash, minor terrain irregularities, and real-time sensor noise. Nonetheless, both controllers successfully ensured stable and consistent tracking, with the ADRC controller showing slightly better compensation in curved motion segments due to its active disturbance estimation capability. Importantly, no significant wheel slip was observed in any of the physical trials, confirming the effectiveness of the vacuum-assisted friction mechanism in maintaining traction, even at higher speeds and during sharp heading changes.

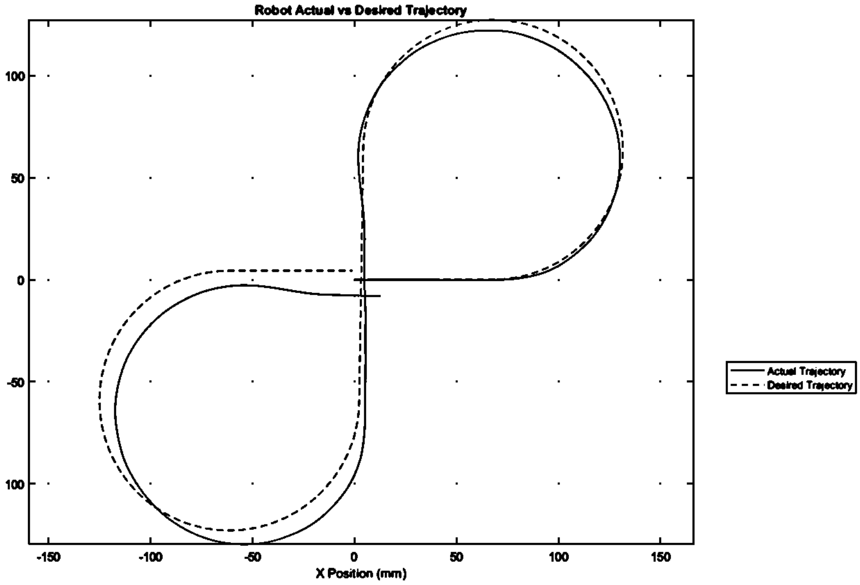

Figure 8. PD controller – Figure-eight trajectory input/output profiles

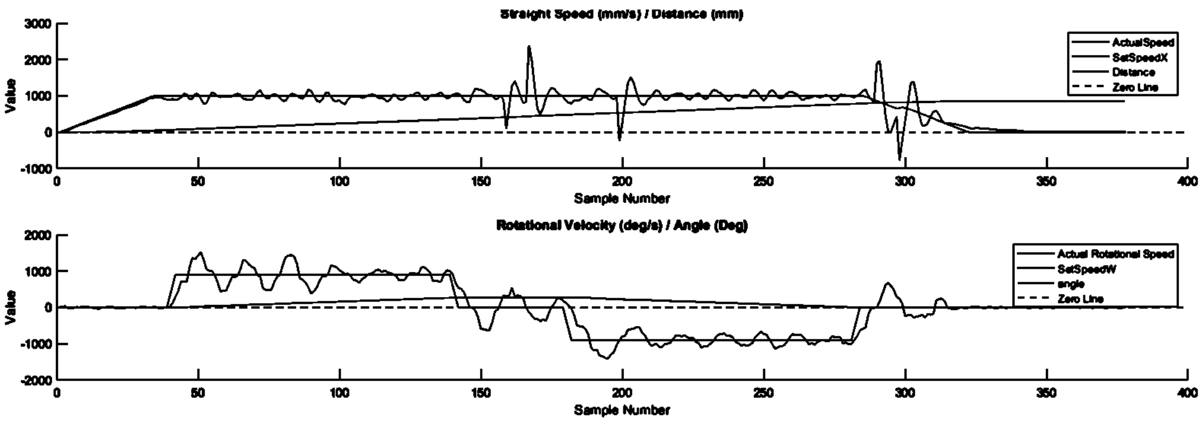

Figure 9. PD controller – (top) Straight Speed (bottom) Angular Speed

Another noteworthy observation was the difference in battery current usage between the two controllers. Although current dynamics were not part of the control model, data was recorded in real-time using a current sensor placed between the battery and motor driver circuitry.

From the results, it can be further compared that saying the PD controller showed slightly higher current fluctuations, especially during sharp directional changes in the figure-eight path (Figure 11 and Figure 12). These peaks suggest momentary instability or overcompensation in control signals. On the other hand, the ADRC controller, on the other hand, demonstrated smoother current profiles with fewer transients, indicating more efficient handling of disturbances and smoother actuation patterns. This difference implies that, beyond improved tracking performance, ADRC may also offer better energy efficiency, although further study is required to confirm this trend under a wider range of motion scenarios and loads. It is important to emphasize that battery current modeling was not included in the simulation. Thus, these current profiles are purely empirical measurements, highlighting an important direction for future work: incorporating energy usage into the control design for energy-aware mobile robot navigation.

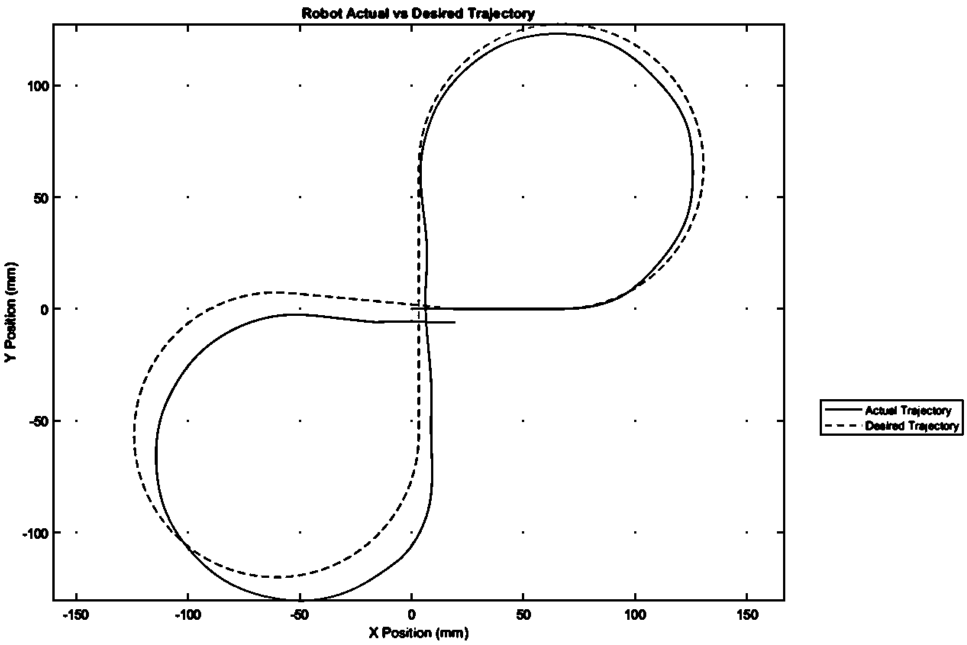

Figure 10. ADRC controller – Figure-eight trajectory input/output profiles

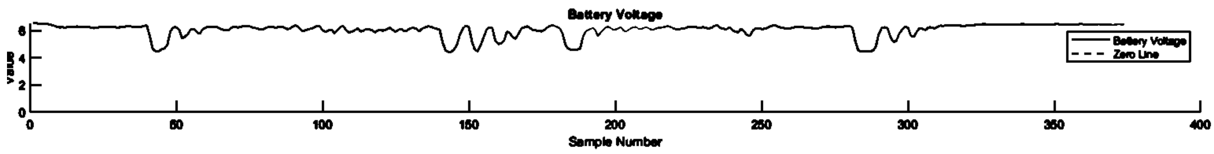

Figure 11: Battery current profile – PD controller

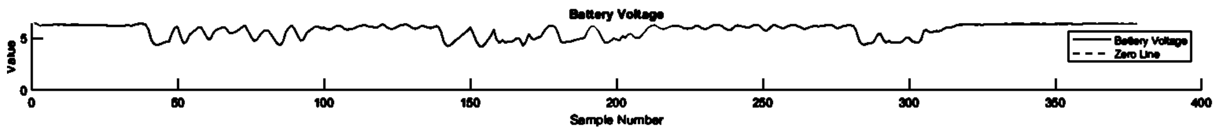

Figure 12: Battery current profile – ADRC controller

CONCLUSION.

This study demonstrated a complete workflow for modeling, control, and validation of a compact mobile robot using a data-driven system identification strategy and two distinct control architectures—PD and ADRC. Simulation and experimental results confirmed that both controllers can achieve accurate trajectory tracking, even with limited hardware resources and unmodeled dynamics. Notably, ADRC showed better performance in curved trajectories, with smoother control effort and improved energy efficiency, as reflected in the reduced battery current fluctuations. By using empirical modeling instead of relying on unavailable datasheets, the research bridges a common gap in the design of affordable mobile robotic platforms. The integration of vacuum-assisted friction enhancement further enabled high-speed operation without slippage, validating the physical robustness of the design.

Future work will address two key limitations: (1) incorporating electrical power consumption into the control framework, and (2) extending validation to a broader range of trajectories and environmental conditions. Additionally, multi-objective optimization combining tracking accuracy and energy usage will be explored for adaptive real-time control.

REFERENCES

[1] Muñoz-Hernandez, G. A., Díaz-Téllez, J., Estevez-Carreon, J., & García-Ramírez, R. S. (2023). ADRC attitude controller based on ROS for a two-wheeled self-balancing mobile robot. *IEEE Access, 11*, 94636–94646. https://doi.org/10.1109/ACCESS.2023.3308948

[2] Ušinskis, V., Nowicki, M., Dzedžickis, A., & Bučinskas, V. (2025). Sensor-fusion based navigation for autonomous mobile robot. *Sensors, 25*(4), 1248. https://doi.org/10.3390/s25041248

[3] Yuan, C., Chang, Y., Song, Y., Lin, S., & Jing, F. (2024). Design and analysis of a negative pressure wall-climbing robot with an omnidirectional characteristic. *Robotica*, Advance online publication.

[4] Norzalilah, N. M., & Samad, Z. (2023). Study of friction compensation model for mobile robot joints. *FME Transactions, 51*(2), 321–330.

[5] Active disturbance rejection control for robotic systems: A review. (2021). *Expert Systems with Applications, 174*, 114772.

[6] Robust ADRC in two-wheeled robots: Experimental study. (2023). *International Conference on Robotics and Mechatronics Proceedings*, 47–52.

[7] Trajectory tracking control for a biomimetic spherical robot. (2021). In *Proceedings of the IEEE International Conference on Mechatronics and Automation* (pp. 951–959).

[8] Robotics perception and control: Key technologies and applications. (2024). *International Journal of Robotics Research, 43*(1), 5–24.

[9] Sensor-fusion based mobile manipulator remote control for smart home. (2025). *arXiv*. https://arxiv.org/abs/2504.13370v1

[10] 3D ToF LiDAR in mobile robotics: A review. (2022). *arXiv*. https://arxiv.org/abs/2202.11025

[11] Hussein, A. K., & Al-Khafaji, H. M. (2022). *Design and Implementation of PID Controller for Path Tracking of Mobile Robot Based on Arduino Microcontroller*. International Journal of Mechanical Engineering and Robotics Research (IJMERR), 11(7), 1235–1240. https://www.ijmerr.com/uploadfile/2022/0708/20220708035145641.pdf

[12] Wu, H., & Cao, C. (2011). *Study on ADRC-based mobile robot lateral control*. In Proceedings of the 30th Chinese Control Conference (pp. 3753–3757). https://www.researchgate.net/publication/224313268_Study_on_ADRC-based_mobile_robot_lateral_control

[13] Han, J. (2009). From PID to Active Disturbance Rejection Control. *IEEE Transactions on Industrial Electronics, 56*(3), 900–906. https://doi.org/10.1109/TIE.2008.2011621

[14] Guffanti, C., Sacco, M., & Cazzaniga, N. E. (2025). *Trajectory tracking wheeled mobile robots through system identification and slip modeling* [Master's thesis, Politecnico di Torino]. Webthesis. https://webthesis.biblio.polito.it/14638/1/tesi.pdf

[15] Masalskyi, V., Dzedžickis, A., Korobiichuk, I., & Bučinskas, V. (2024). Hybrid Mode Sensor Fusion for Accurate Robot Positioning. *Sensors, 24*(9), 2849. https://www.mdpi.com/1424-8220/24/9/2849